Proceedings of the Canadian Society for Mechanical Engineering International Congress 2021
CSME Congress 2021
June 27-30, 2021, Charlottetown, PE, Canada

ULTRASONIC SPOT WELDING OF ALUMINUM ALLOYS WITH AND WITHOUT ALCLAD LAYER

S.M.A.K. Mohammed[1*], S.S. Dash[1], A. Albedah[2], X.Q. Jiang[3], D.Y. Li[4], D.L. Chen[1]
[1]Department of Mechanical and Industrial Engineering, Ryerson University, 350 Victoria Street, Toronto, Ontario M5B 2K3, Canada
[2]Mechanical Engineering Department, College of Engineering, King Saud University, PO Box 800, Riyadh 11421, Saudi Arabia
[3]School of Materials and Energy, Southwest University, Tiansheng Road 2, Beibei District, Chongqing 400715, China
[4]Department of Chemical and Materials Engineering, University of Alberta, AB T6G 1H9, Canada
*sohail@ryerson.ca

Abstract—Solid-state ultrasonic spot welding (USW) of AA5182-AA5182 and Alclad AA7075-AA7075 was performed to evaluate the microstructural features at weld interface, joint robustness and the static and fatigue properties. Strong and defect-free joints were attained in both aluminum alloys via USW. High temperatures at the weld interface were rapidly reached especially at high welding energy levels, which facilitated the weldability of joints. The microstructure of the weld interface evaluated via electron backscatter diffraction (EBSD) exhibited a necklace-like characteristic with fine grains, manifesting the attainment of robust bonding. The obtained tensile lap shear failure load increased with increasing welding energy, with a maximum of ~6 kN satisfied the requirement of AWS D17.2 standards. Furthermore, the welded joints of both alloys exhibited a superior fatigue resistance, with the so-called "unweldable" AA7075 having a fatigue life even somewhat longer than that of AA5182, which was associated with the existence of softer AA7072 Alclad layer. The results obtained in this study demonstrated that USW is a promising solid-state welding technique with shorter weld cycles and high energy-efficiency, which can be used for joining thin sheets in the automotive applications.

Keywords-Aluminum alloys; Alclad; ultrasonic spot welding; tensile lap shear; fatigue.

I. INTRODUCTION

The challenge of climate change is propelling the transportation industry towards more fuel-efficient products and manufacturing processes with lower energy consumption [1]. This inevitably entails the fabrication and/or joining of lightweight body structures. The transportation industry has emphasized the demand for efficient joining methods to boost the flexibility of design. Ultrasonic spot welding (USW) is one of the emerging solid-state welding processes, producing robust joints with low energy consumption [2]–[5]. The USW works based on the principle of converting electrical energy to mechanical vibrations at a high frequency normally at 20 kHz. Short weld cycle time (~0.5-1 s) results in strong welded joints owing to a small heat-affected zone (HAZ) [6], [7]. A strong USW joint could be obtained at a welding energy as low as 0.6 kJ, compared with the required high welding energy of 50-100 kJ by resistance spot welding [3]. Several studies demonstrated the benefits of USW compared to conventional techniques, and reported the increase in tensile properties of the joint with increasing welding energy [8]–[11]. The high temperature generated during USW facilitates the weldability of aluminum alloy (AA) joints [12]. The feasibility of USW of body structures with promising results was validated by Ford Motor Company [7]. Aluminum alloys like AA5182 have been commonly used for manufacturing vehicle body, brackets, etc., and thus became prominent candidate alloys for joining-related applications, while some aluminum alloys like AA7075 mostly used in the aerospace applications are difficult to be welded by fusion welding and termed as "unweldable" [13]. Recently, we have reported a defect-free and robust bonding of AA7075-AA7075 via USW [14], with the presence of Alclad coating, which is also referred to as corrosion resistant alloy (CRA).

The aim of the present study was to identify and compare the feasibility of joining AA5182-AA5182 and Alclad AA7075-AA7075 via USW. The interfacial microstructure, static strength and fatigue life of the joints were evaluated over a wide range of welding energies in relation to the temperature at the weld center.

II. METHODOLOGY

AA5182-H19 (Al-4.5Mg-0.35Mn) and AA7075-T6 (Al-5.7Zn-2.5Mg-1.4Cu) sheets of 2 mm thick were used in the present study. The sheets of AA7075 were cladded with a ~50 µm CRA which was AA7072 (Al-1Zn) by metallurgical bonding on both sides. The sheets were machined into 20mm×15mm and 80mm×15mm strips, with the length being in the rolling direction (RD), for the temperature measurement

and microstructural characterization, and for the determination of mechanical properties, respectively. USW was performed on MH2016 dual-wedge reed Sonobond HP ultrasonic spot welder in an energy-controlled mode as schematically shown in Fig. 1. The transverse vibration direction of the upper and lower sonotrode tips regulated by respective transducers should be reverse, i.e., with a phase shift of 180°, aiming to maximize the amplitude. The welding parameters include ultrasonic vibration frequency (f) of 20 kHz, maximum power output (P) of 2 kW and a clamping pressure of 0.4 MPa. The optimum impedance setting of 2 and 8 is implemented for AA5182 and AA7075, respectively. The welding energies of as low as 500 J to a maximum of 6000 J were applied in the present study. The sample preparation and welding process could be found elsewhere [14], [15].

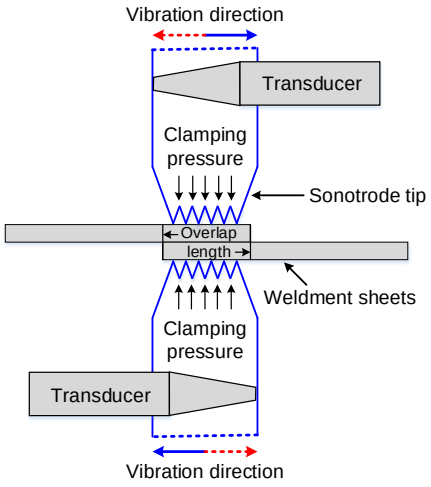

Figure 1. Schematic illustration of USW test setup.

A small groove was machined on the faying surface of 20mm×15mm to accommodate the K-type thermocouple (diameter = 0.076 mm) for temperature measurements. The microstructures and fracture surfaces of the joints were observed using a scanning electron microscope (SEM) equipped with energy-dispersive X-ray spectroscopy (EDS) and electron backscatter diffraction (EBSD). EBSD was performed on the sectioned samples welded at 4000 J. The EBSD samples were ground using SiC papers ranging from #600 to #4000 and polished with diamond paste down to 0.5 µm, followed by electropolishing in an electrolyte containing 90% ethanol and 10% perchloric acid at 20 V for ~20 s at room temperature. The analyses were conducted at a working distance of 15 mm, a fixed voltage of 20 kV, and a tilt angle of 70° in SEM. The fracture surface of the selected samples was observed to identify the fracture mechanisms.

The tensile and fatigue specimens were welded with an overlap length of 20 mm. The tensile tests were performed with the samples welded at different welding energies at a displacement rate of 1mm/min on the United tensile testing machine. Samples welded at 4000 J were used to perform stress-controlled fatigue tests at a load ratio R ($=P_{min}/P_{max}$) of 0.2 and sinusoidal waveform with a frequency of 50 Hz on Instron 8801 servo-hydraulic testing system at various maximum cyclic loads ranging from 0.5 kN to 5 kN. Tension-tension cyclic loading was adapted to avoid any potential buckling during the tests. Two spacers of 35×15×2 mm machined from the same material were attached to prevent the effect of rotation and asymmetric bending moment during the fatigue tests.

III. Results and Discussions

A. *Temperature measurements*

The average peak temperature at the center of the weld for both AA5182 and Alclad AA7075 was measured and presented as a function of welding energy in Fig. 2(a). A similar quick increase in temperature could be observed in both alloys as the welding energy increased. A close examination indicated that a higher welding temperature could be achieved in the Alclad AA7075 especially in the welding energy range below ~2000 J due to the presence of a softer AA7072 (Al-1Zn) surface layer, while the welding temperature in both alloys was equivalent in the welding energy range above ~2000 J within the experimental scatter. The average peak temperature in AA5182 raised from 235°C at 1000 J to ~522°C at 4000 J; and from ~242°C at 500 J to a maximum of ~513°C at 3000 J in AA7075 joints. A peak temperature of >500°C recorded in both alloys is still below the liquidus temperature of respective alloys which confirms that the welding occurred in a solid-state condition. Obviously, such high temperatures generated via the high-frequency vibration (or surface rubbing) during USW are responsible for softening the weld zone that is needed for joining, but also for the plastic deformation between the sonotrode tips accompanied by clamping pressure.

B. *Microstructural evolution*

The EBSD orientation map of the cross-section of AA5182 and Alclad AA7075 welded at 4000 J is presented in Fig. 2(b) and (c), respectively. The diagonal lower and upper half corresponds to the orientation map and recrystallization fraction map, respectively, in both Fig. 2(b) and (c). It is observed that both alloys were well joined via USW without visible defects along the weld interface oriented horizontally in Fig. 2(b) and (c). In general, in the base metal (BM) the grain size of AA5182 was smaller than that of the Alclad AA7075. Further grain refinement was observed in the weld zone of both alloys due to the occurrence of dynamic recrystallization (DRX) during USW. However, the grains in the BM retained their elongated nature in the rolling direction due to a smaller HAZ formed in short USW cycles (~0.5-1 sec), along with the retainment of the Alclad layer in AA7075. The retainment of Alclad layer was verified by microstructural observations along with EDS analyses. The difference in grains in the weld zone and BM was attributed to the difference in temperature which was higher at the weld interface stemming from ultrasonic vibrations and plastic deformation at a high strain rate during welding. The width of the weld zone in AA5182 was ~30 µm whereas it was larger in Alclad AA7075 (Fig. 2(c)). This would be related to the presence of the initially ~50 µm thick Alclad layer on both upper and lower sheets, which was also softer [14].

The necklace-like DRX band at the interface infers that the temperatures during welding exceeded the recrystallization

temperature of Al alloys (340°C-400°C) [16], which was corroborated from the temperature measurements in Fig. 2(a). The fraction of recrystallized grains in the weld zone of AA5182 was higher whereas deformed grains dominated the weld zone of AA7075 joins which is again associated with the softer Alclad layer. Fewer substructured grains appeared in the weld zone of both alloys. Furthermore, the presence of DRX in the weld zone suggests that the bonding would be robust. To confirm this, the tensile lap shear test results are presented in next section.

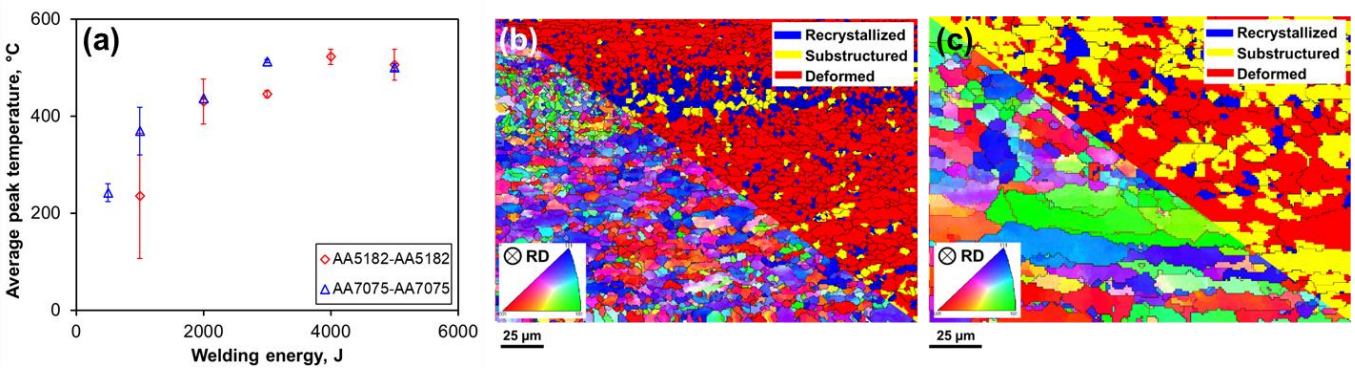

Figure 2. (a) The peak welding temperature measured at different welding energies; EBSD orientation maps (bottom left) and the evolution of grains (top right) of (b) AA5182-AA5182 and (c) AA7075-AA7075 welded at 4000 J.

C. Tensile properties

The tensile lap shear failure load, critical stress intensity factor (K_c) and total failure energy of the USWed AA5182 and Alclad AA7075 are presented in Fig. 3(a) and (b). The failure load increased with increasing welding energy for both alloys and surpassed the requirement of AWS D17.2 standards for the spot-welded sheet specimens at higher welding energies. It is appealing that the so-called unweldable AA7075 even outperformed AA5182 marginally at some welding energies. Moreover, the failure load of the present alloys was in general much higher than several other aluminum alloy joints [6], [17]. It should be noted that in the Alclad AA7075 at the higher welding energy, due to higher welding temperatures generated (Fig. 2(a)) and more severe plastic deformation, the softer Alclad metal squeezed into the voids at the ends of the interface, leading to the formation of additional microbonds and the reduction of stress concentration there. As a result, the tensile lap shear failure load appeared to keep increasing within the applied welding energy range up to 6000 J. However, this trend could not be sustained if further higher energies would be applied due to the further sample thinning in-between the sonotrode tips.

Macwan *et al.* [18] pointed out that the decrease in the tensile lap shear failure load of the welded joints at higher welding energies was closely related to the welding tip penetration (or sample thinning). In general, as the welding energy increased, the microbond density increased, accompanied by an increased penetration as well. Thus, the failure load increased until a threshold was reached followed by a reduction. This phenomenon is common in several USWed joints [18]–[20]. In contrast, the lap shear load of USWed Alclad AA7075 in the present study exhibited increasing failure load with increasing welding energy up to 6000 J. This was directly related to the presence of the softer Alclad layer on the surface of AA7075 sheets, as discussed above.

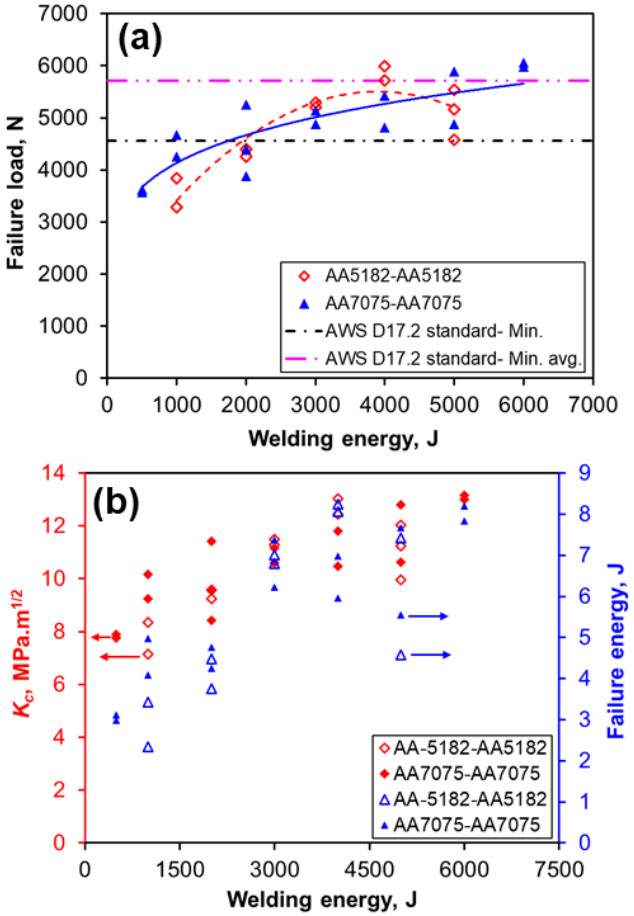

Figure 3. (a) Tensile lap shear failure load, and (b) critical stress intensity factor (K_c) and failure energy of the USWed AA5182-AA5182 and Alclad AA7075-AA7075 joints as a function of welding energy.

Fig. 2(b) presents the change of failure energy and critical stress intensity factor, K_c, with welding energy, which could be calculated based on the following equation [21],

$$K_c = 0.694 F_t / d\sqrt{t}\,, \quad (1)$$

where F_t is the peak tensile load, d is the nugget diameter, and t is the sheet thickness. The parameters used in the calculation were detailed in [14], [15].

The failure energy is defined as the area under the tensile test curve, which could be used to better indicate the effect of welding energy. The value of K_c and failure energy increased with increasing welding energy similar to the failure load in Fig. 3(a). Alclad AA7075 exhibited higher values of K_c and failure energy than AA5182 especially in the lower welding energy range, with a maximum K_c and failure energy of 13.2 MPa-m$^{1/2}$ and 8.0 J at a welding energy of 6000 J. These results further corroborated robust bonding generated via USW, demonstrating that the process is promising and helps pave the way for some automotive applications, provided that the joints could withstand cyclic loading which will be presented in next section.

D. *Fatigue properties*

Fig. 4 illustrates a plot between the maximum cyclic load versus the number of cycles to failure (S-N curve), which is a measure of the lap shear fatigue life. The samples welded at an energy of 4000 J were selected for fatigue tests. The run-out data points for the sampled without failure beyond 1×10^7 cycles were labeled with horizontal arrows. The fatigue life of both alloys increased with decreasing applied maximum cyclic load. The Alclad AA7075 exhibited marginally better fatigue resistance than AA5182 which was associated with the better bonding of softer Alclad alloy AA7072 (Fig. 2(c)) and tensile properties (Fig. 3(a)).

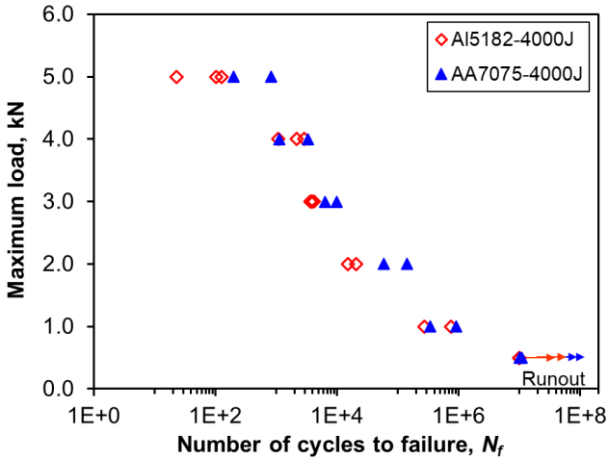

Figure 4. S-N curves of AA5182- AA5182 and Alclad AA7075-AA7075 joints USWed at 4000 J, R = 0.2 and frequency = 50 Hz.

Although the failure load of AA5182 was slightly higher than Alclad AA7075 at a welding energy of 4000 J, the overall tensile properties of Alclad AA7075 were better which led to a slight increase in fatigue properties. The fatigue strength of the welded joints was also related to the tensile strength of the BM [22], which was higher in Alclad AA7075. Furthermore, the improved fatigue life was also associated with the potential squeezed-out effect at the higher welding energy level and temperature, which led to the formation of additional microbonds and the reduction of stress concentration there, as discussed earlier. The USWed joints of both alloys exhibited a superior fatigue resistance compared to the welded joints of several other aluminum alloys [6], [17]. Again, a widely used AA7075 which has been challenging to be welded by fusion processes could be well joined via USW due to the presence of softer AA7072 Alclad layer, with promising results and superior resistance than several weldable aluminum alloys.

E. *Fractography*

Fig. 5 presents the fatigue fracture surfaces of AA5182 and AA7075 alloys welded at 4000 J, fatigued at P_{max} = 5 kN. The fatigue failure was in the form of interfacial failure. There were multiple crack initiation sites, and the crack propagation regions are presented in Fig. 5(a) and (b) for AA5182 and AA7075 welded joints, respectively. There were very faint fatigue striations present on the fracture surface of AA5182, but clear fatigue striations were present on the fracture surface of AA7075, further demonstrating the robust bonding along with a larger plastic zone ahead of the crack tip due to the presence of softer AA7072 Alclad layer. Fig. 5(c) and (d) depicts the fast fracture regions for AA5182 and AA7075 welded joints, respectively, which showed the ductile behavior of the welded joints. The presence of sheared, non-closure dimples on the fracture surface indicated ductile deformation in well-joined lap shear type samples for both alloys. The presence of finer dimples in Fig. 5(d) than Fig. 5(c) appeared to demonstrate that AA7075 welded joints were more ductile than AA5182 welded joints, also indicating better bonding.

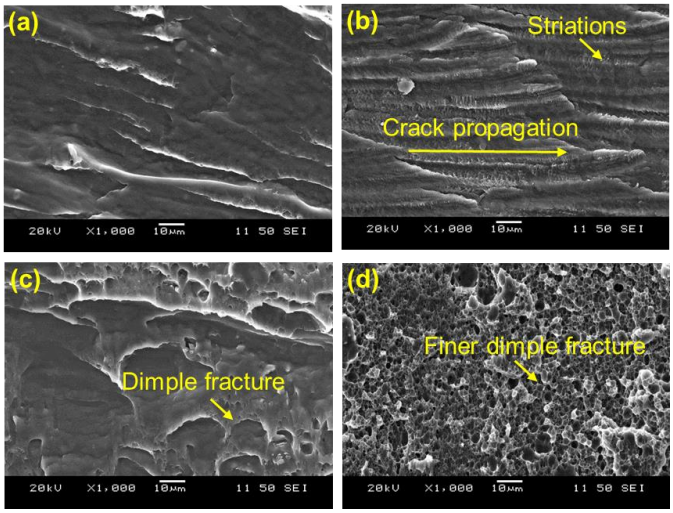

Figure 5. Fatigue fracture surface of (a) AA5182 and (b) AA7075 welded joints; dimpled fast-fracture region for (c) AA5182 and (d) AA7075, where all the samples were welded at 4000 J and failed at P_{max} = 5 kN.

IV. CONCLUSIONS

A robust bonding with superior static and fatigue properties was achieved via ultrasonic spot welding of AA5182 and

AA7075. The interfacial temperature increased with increasing welding energy, with temperatures greater than 500 °C recorded at high welding energies. A "necklace"-like grain structure was observed along the weld zone as a result of dynamic crystallization, which occurred due to severe plastic deformation and high temperatures during welding. The tensile lap shear failure load reached a maximum of ~6 kN and surpassed the requirement by AWS D17.2 standards at higher welding energies in both alloys. The increase in the temperature at higher welding energy beyond 4000 J led to a decrease in the failure load of AA5182 welded joints, whereas the failure load continued to increase in Alclad AA7075 due to the soft nature of AA7072 Alclad layer. The fatigue resistance of Alclad AA7075 welded joints was observed to be higher than AA5182 welded at 4000 J at a given applied cyclic load. These results demonstrated that the so-called "unweldable" AA7075 could be well-joined by this solid-state USW technique with superior mechanical properties, as long as it contained a softer Alclad layer.

ACKNOWLEDGMENT

The authors would like to thank the Natural Sciences and Engineering Research Council of Canada (NSERC), Deanship of Scientific Research at King Saud University (research group No. RGP-VPP-035) and Natural Science Foundation of China (NSFC) (Grant No. 51475385) in the form of international research collaboration. The authors would also like to thank Messrs. Q. Li, A. Machin, J. Amankrah and R. Churaman for easy access to the laboratory facilities of Ryerson University and their assistance in the experiments.

REFERENCES

[1] B. K. Sovacool *et al.*, "Sustainable minerals and metals for a low-carbon future," *Science.*, vol. 367, no. 6473, pp. 30–33, Jan. 2020, doi: 10.1126/science.aaz6003.

[2] W. Zhang *et al.*, "On the metallurgical joining mechanism during ultrasonic spot welding of NiTi using a Cu interlayer," *Scr. Mater.*, vol. 178, pp. 414–417, Mar. 2020, doi: 10.1016/j.scriptamat.2019.12.012.

[3] D. Bakavos and P. B. Prangnell, "Mechanisms of joint and microstructure formation in high power ultrasonic spot welding 6111 aluminium automotive sheet," *Mater. Sci. Eng. A*, vol. 527, no. 23, pp. 6320–6334, Sep. 2010, doi: 10.1016/j.msea.2010.06.038.

[4] V. K. Patel, S. D. Bhole, and D. L. Chen, "Influence of ultrasonic spot welding on microstructure in a magnesium alloy," *Scr. Mater.*, vol. 65, no. 10, pp. 911–914, Nov. 2011, doi: 10.1016/j.scriptamat.2011.08.009.

[5] J. E. Gould, "Joining aluminum sheet in the automotive industry—A 30 year history," *Weld. J.*, vol. 91, no. 1, p. 23, 2012.

[6] H. Peng, D. L. Chen, and X. Q. Jiang, "Microstructure and mechanical properties of an ultrasonic spot welded aluminum alloy: The effect of welding energy," *Materials*, vol. 10, no. 5, p. 449, Apr. 2017, doi: 10.3390/ma10050449.

[7] R. Jahn, R. Cooper, and D. Wilkosz, "The effect of anvil geometry and welding energy on microstructures in ultrasonic spot welds of AA6111-T4," *Metall. Mater. Trans. A*, vol. 38, no. 3, pp. 570–583, Apr. 2007, doi: 10.1007/s11661-006-9087-0.

[8] T. Wang, S. Sinha, M. Komarasamy, S. Shukla, S. Williams, and R. S. Mishra, "Ultrasonic spot welding of dissimilar Al 6022 and Al 7075 alloys," *J. Mater. Process. Technol.*, vol. 278, p. 116460, Apr. 2020, doi: 10.1016/j.jmatprotec.2019.116460.

[9] F. A. Mirza, A. Macwan, S. D. Bhole, D. L. Chen, and X. G. Chen, "Microstructure, tensile and fatigue properties of ultrasonic spot welded aluminum to galvanized high-strength-low-alloy and low-carbon steel sheets," *Mater. Sci. Eng. A*, vol. 690, pp. 323–336, 2017, doi: 10.1016/j.msea.2017.03.023.

[10] Z. L. Ni and F. X. Ye, "Ultrasonic spot welding of aluminum alloys: A review," *J. Manuf. Process.*, vol. 35, pp. 580–594, Oct. 2018, doi: 10.1016/j.jmapro.2018.09.009.

[11] V. K. Patel, S. D. Bhole, and D. L. Chen, "Friction stir spot and ultrasonic spot welding of dissimilar magnesium-to-aluminum alloys," *Proc. 24th CANCAM*, pp. 6–9, 2013.

[12] Z. L. Ni and F. X. Ye, "Ultrasonic spot welding of Al sheets by enhancing the temperature of weld interface," *Mater. Lett.*, vol. 208, pp. 69–72, Dec. 2017, doi: 10.1016/j.matlet.2017.05.009.

[13] M. Sokoluk, C. Cao, S. Pan, and X. Li, "Nanoparticle-enabled phase control for arc welding of unweldable aluminum alloy 7075," *Nat. Commun.*, vol. 10, no. 1, p. 98, Dec. 2019, doi: 10.1038/s41467-018-07989-y.

[14] S. M. A. K. Mohammed, Y. D. Jaya, A. Albedah, X. Q. Jiang, D. Y. Li, and D. L. Chen, "Ultrasonic spot welding of a clad 7075 aluminum alloy: Strength and fatigue life," *Int. J. Fatigue*, vol. 141, p. 105869, Dec. 2020, doi: 10.1016/j.ijfatigue.2020.105869.

[15] S. M. A. K. Mohammed, S. S. Dash, X. Q. Jiang, D. Y. Li, and D. L. Chen, "Ultrasonic spot welding of 5182 aluminum alloy: Evolution of microstructure and mechanical properties," *Mater. Sci. Eng. A*, vol. 756, pp. 417–429, 2019, doi: 10.1016/j.msea.2019.04.059.

[16] R. Singh, *Applied Welding Engineering: Processes, Codes, and Standards*, 2nd Ed. Butterworth-Heinemann, 2015.

[17] F. A. Mirza, A. Macwan, S. D. Bhole, and D. L. Chen, "Microstructure and fatigue properties of ultrasonic spot welded joints of aluminum 5754 alloy," *JOM*, vol. 68, no. 5, pp. 1465–1475, May 2016, doi: 10.1007/s11837-015-1796-7.

[18] A. Macwan, F. A. Mirza, S. D. Bhole, and D. L. Chen, "Similar and dissimilar ultrasonic spot welding of 5754 aluminum alloy for automotive applications," *Mater. Sci. Forum*, vol. 877, pp. 561–568, Nov. 2016, doi: 10.4028/www.scientific.net/MSF.877.561.

[19] F. A. Mirza, A. Macwan, S. D. Bhole, D. L. Chen, and X. G. Chen, "Effect of welding energy on microstructure and strength of ultrasonic spot welded dissimilar joints of aluminum to steel sheets," *Mater. Sci. Eng. A*, vol. 668, pp. 73–85, 2016, doi: 10.1016/j.msea.2016.05.040.

[20] H. Peng, X. Q. Jiang, X. F. Bai, D. T. Li, and D. L. Chen, "Microstructure and mechanical properties of ultrasonic spot welded Mg/Al alloy dissimilar joints," *Metals*, vol. 8, no. 4, pp. 229, Apr. 2018, doi: 10.3390/met8040229.

[21] S. Zhang, "Stress intensities at spot welds," *Int. J. Fract.*, vol. 88, no. 2, pp. 167–185, 1997, doi: 10.1023/A:1007461430066.

[22] J. A. Davidson and E. J. Imhof, "The effect of tensile strength on the fatigue life of spot-welded sheet steels," SAE Transactions, vol. 93, pp. 660-669, 1984, doi: 10.4271/840110.